Acta Pharmaceutica Sinica B 2024;14(5):2247–2262

Chinese Pharmaceutical Association
Institute of Materia Medica, Chinese Academy of Medical Sciences

Acta Pharmaceutica Sinica B

www.elsevier.com/locate/apsb
www.sciencedirect.com

ORIGINAL ARTICLE

Radiation-based immunogenic vaccine combined with a macrophage "checkpoint inhibitor" for boosting innate and adaptive immunity against metastatic colon cancers

Hongbo Xu[a], Xianya Qin[a], Yuanyuan Guo[c], Siyu Zhao[a], Xingxing Feng[a], Runzan Zhang[a], Tianyi Tian[a], Li Kong[a,*], Conglian Yang[a,*], Zhiping Zhang[a,b,*]

[a]*Tongji School of Pharmacy, Huazhong University of Science and Technology, Wuhan 430030, China*
[b]*Hubei Engineering Research Center for Novel Drug Delivery System, Wuhan 430030, China*
[c]*Wuhan Liyuan Hospital of Tongji School of Pharmacy, Huazhong University of Science and Technology, Wuhan 430077, China*

Received 17 October 2023; received in revised form 8 December 2023; accepted 16 December 2023

KEY WORDS

Immunogenic cell death;
Cancer vaccine;
X-ray;
Efferocytosis;
Macrophage;
STING;
Adaptive immunity;
Innate immunity

Abstract Immunogenic dying tumor cells hold promising prospects as cancer vaccines to activate systemic immunity against both primary and metastatic tumors. Especially, X-ray- induced dying tumor cells are rich in highly immunogenic tumor-associated antigens and self-generated dsDNA as potent adjuvants. However, we found that the X-ray induction process can result in the excessive exposure of phosphatidylserine in cancer vaccines, which can specifically bind with the MerTK receptor on macrophages, acting as a "checkpoint" to facilitate immune silence in the tumor microenvironment. Therefore, we developed a novel strategy combining X-ray-induced cancer vaccines with UNC2250, a macrophage MerTK "checkpoint inhibitor," for treating peritoneal carcinomatosis in colon cancer. By incorporating UNC2250 into the treatment regimen, immunosuppressive efferocytosis of macrophages, which relies on MerTK-directed recognition of phosphatidylserine on vaccines, was effectively blocked. Consequently, the immune analysis revealed that this combination strategy promoted the maturation of dendritic cells and M1-like repolarization of macrophages, thereby simultaneously eliciting robust adaptive and innate immunity. This innovative approach utilizing X-ray-induced vaccines combined with a checkpoint inhibitor may provide valuable insights for developing effective cancer vaccines and immunotherapies targeting colon cancer.

*Corresponding authors.
E-mail addresses: kongl@hust.edu.cn (Li Kong), conglianyang@hust.edu.cn (Conglian Yang), zhipingzhang@mail.hust.edu.cn (Zhiping Zhang).
Peer review under the responsibility of Chinese Pharmaceutical Association and Institute of Materia Medica, Chinese Academy of Medical Sciences.

https://doi.org/10.1016/j.apsb.2024.02.015

1. Introduction

Peritoneal carcinomatosis is a fatal clinical manifestation in the late-stage of colon cancer (PCCC), with a remarkably poor prognosis[1,2]. Unfortunately, conventional treatment strategies, including cytoreductive surgery therapy, hyperthermic intraperitoneal chemotherapy, radiotherapy, and immune checkpoint blockade therapy, have shown limited efficacy in managing PCCC due to rapid metastasis and immunosuppressive microenvironment[2-6]. For metastatic colon cancer, cancer vaccines have been regarded as an effective strategy. Particularly, vaccine systems based on immunogenic dying tumor cells (DTC) and their components induced by specific immunogenic cell death (ICD) inducers have gained enormous attention[7,8]. Hence, developing a safer and effective cancer vaccine based on DTC may provide a reliable solution for the therapy of metastatic PCCC.

Our previous work proved the effectiveness of DTC vaccines induced by chemotherapeutic drugs like doxorubicin in eliciting robust immune response[9]. Besides chemotherapeutic drugs, X-radiation can also induce potent ICD in tumor cells, thus improving the immunogenicity of DTC. Nevertheless, unlike chemotherapeutic drugs, DTC induced by X-radiation could completely circumvent the side effects on the immune system caused by residual cytotoxic drugs. More importantly, severe DNA damage induced by X-ray can result in abnormal accumulation of double-strand DNA (dsDNA) in the cytoplasm of DTC[10]. These cytoplasmic dsDNA can serve as a potent adjuvant to activate the stimulator of interferon genes (STING) signal in antigen presentation cells (APCs), thus triggering a robust type-I interferon response to potentiate antitumor immunity[11-14]. Compared to chemotherapeutic drugs, X-ray is a more effective and safer ICD inducer. Of note, the immunogenicity and degree of DNA damage in tumor cells were closely related to the dose of X-radiation. Recent research has proved that repeated low-dose radiation *in situ* can elicit more severe DNA damage and dsDNA content within tumor cells compared with single high-dose radiation[14]. However, the precise dose-effect relationship between *in vitro* X-radiation dose and immunogenicity remained unclear for DTC induction. Therefore, future investigations should focus on elucidating this relationship comprehensively to maximize therapeutic efficacy for DTC induced by X-radiation.

To enhance the efficiency of the DTC vaccine, regular synergetic strategies tend to combine with adjuvants to promote the activation of dendritic cells (DCs), thus eliciting stronger adaptive immunity. Additionally, macrophages play a vital role in innate immunity, which is assignable. In this work, we found that the procedure of vaccine preparation can excessively flip over phosphatidylserine (PS) on DTC vaccine, which can specifically bind with MER proto-oncogene tyrosine kinase (MerTK) receptor on macrophages, facilitating immunosuppressive clearance of DTC in TME. This process, known as efferocytosis, is the primary factor precluding M1-like polarization of macrophage and antigen presentation to support immune evasion[15]. More importantly, recent research has found that inhibition of MerTK-mediated efferocytosis can lead to a permissive environment for the release and transfer of cGAMP and dsDNA from DTC to macrophage, thereby activating STING pathway and subsequent type I interferon response in macrophages[11,16,17]. Based on these findings, it can be inferred that the MerTK receptor on macrophages can be recognized as the specific immune checkpoint hindering the effectiveness of DTC vaccines. Therefore, MerTK inhibitors may be a potential candidate for adjuvant to improve the therapeutic efficacy of DTC vaccines against metastatic colon cancer.

In this work, we designed an X-ray-induced frozen dying tumor cell (FDT) vaccine to treat PCCC. Firstly, we investigated the correlation between *in vitro* radiation dose and the vaccine's immunogenicity to optimize the radiation dose for the preparation of FDT. Secondly, the FDT vaccine was combined with MerTK inhibitor UNC2250, which served as a "checkpoint inhibitor" of macrophages to relieve immune suppression. After intraperitoneal administration, the FDT vaccine can significantly inhibit tumor growth and malignant ascites in the peritoneal cavity and induce the maturation of DCs effectively to elicit massive infiltration of T lymphocytes and B lymphocytes within tumors. When combined with UNC2250, FDT triggered a potent type I interferon response and simultaneously facilitated the activation of DCs and M1-like polarization of tumor-associated macrophages (TAMs). As a result, this combinational strategy triggered massive apoptosis within tumors and significantly enhanced therapeutic efficiency compared with monotherapy with FDT vaccination. Overall, our findings demonstrate that an X-ray-induced FDT vaccine coupled with a novel synergistic approach targeting macrophage-mediated immunosuppressive clearance holds promise as a therapeutic avenue for improving clinical outcomes in metastatic colon cancer (see Scheme 1).

2. Materials and methods

2.1. Materials and reagents

UNC2250 was purchased from Adooq Bioscience (Nanjing, China). Oxaliplatin and irinotecan were purchased from MedChemexpress (Wuhan, China). Cytometric Beads for cytokine detection were purchased from BD Bioscience (Shanghai, China). BD Biosciences (Shanghai, China). DiD was purchased from Beyotime Biotechnology (Shanghai, China). Granulocyte/macrophage-colony stimulating factor (GM-CSF) was purchased from Dakewe (Shenzhen, China). Macrophage-colony stimulating factor (M-CSF) was purchased from Abcolonal (Wuhan, China), NGS™ dsDNA HS Assay Kit was purchased from Wuhan ABP-Biosciences Co., Ltd. (Wuhan, China). Gibco DMEM medium and Gibco RPMI 1640 medium were purchased from Thermo Fisher Scientific Co., Ltd. (Shanghai, China). Anti-γ H2A.X (phospho S139) antibody was purchased from Abcam (Shanghai, China). STING (D2P2F) Rabbit mAb was purchased from Cell Signaling Technology (Shanghai, China). Phospho-STING

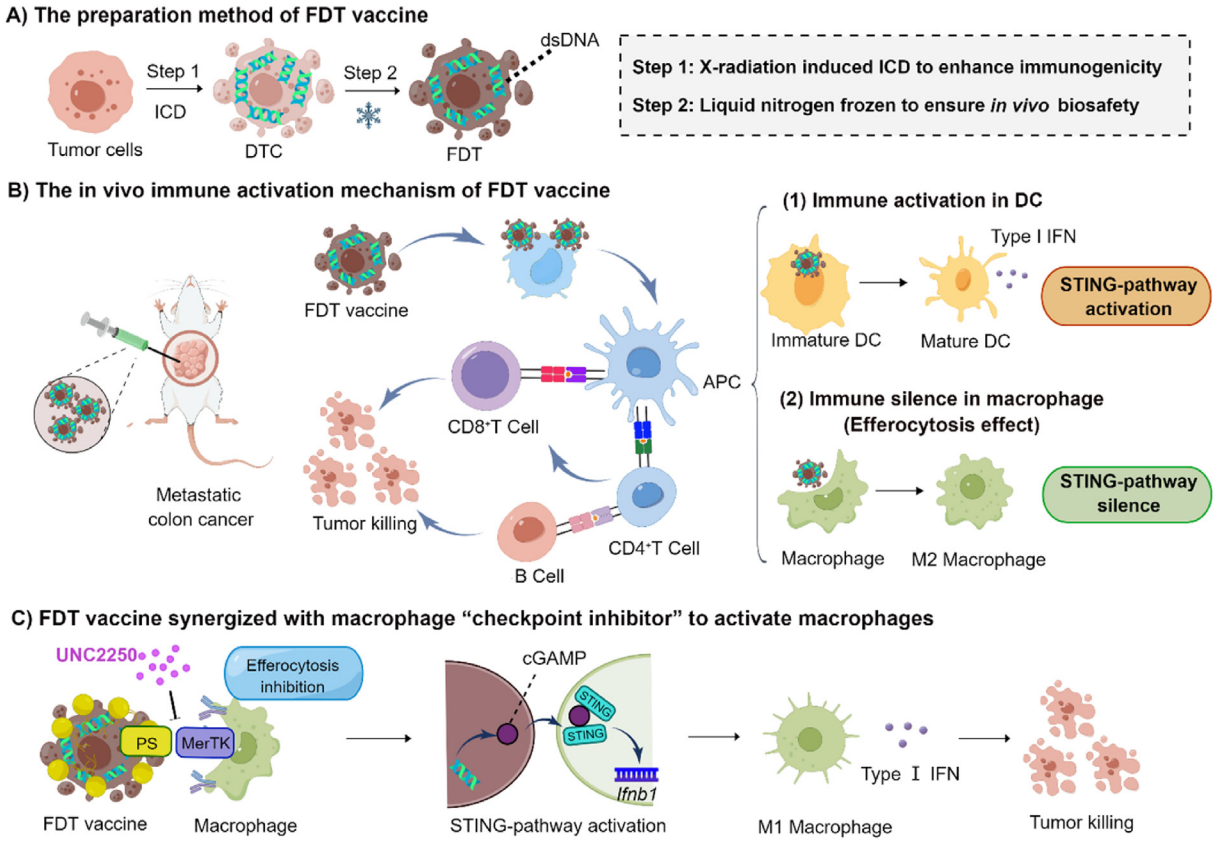

Scheme 1 Schematic illustration of FDT vaccine with the ability to activate systemic immunity for tumor inhibition. (A) FDT vaccines are prepared with X-ray-induced ICD effect and liquid nitrogen cryogenic freezing technology. (B) Benefiting from X-Ray-induced excessive dsDNA accumulation in the cytoplasm of FDT, this FDT vaccine can activate the STING signaling pathway and the maturation of DCs, thus eliciting robust adaptive immunity in the tumor microenvironment. (C) Furthermore, when combined with the inhibitor of efferocytosis (UNC2250), the immune-suppressive clearance of FDT by macrophages was largely decreased, which in turn reprogrammed pro-inflammatory activation of macrophages and finally resulted in double activation of adaptive immunity and innate immunity. The diagrammatic drawing was created by Figdraw.

(Ser365) (D8F4W) Rabbit mAb was purchased from Cell Signaling Technology (Shanghai, China).

2.2. *Cell lines and animals*

MC3 from the C57BL/6 mouse and CT26 cells from the BALB/c mouse were purchased from the Cell Bank of the Chinese Academy of Science (Shanghai, China). Cells were cultivated using Gibco DMEM medium (MC38) or RPMI 1640 medium (CT26) containing 10% fetal bovine serum (FBS) and 1% Penicillin−Streptomycin solution under conditions of 5% CO_2 and 37 °C incubator. The 6−8 weeks female C57BL/6 and BALB/c mice were purchased from the Biotechnology Research Center of Chain Three Gorges University (Yi Chang, China). All animals were fed and experimented according to the guidelines of Laboratory Animals Ethics of Huazhong University of Science and Technology (HUST). The investigators received the assigned [2021] IACUC Number: 3376 from the Institutional Animal Care and Use Committee at Tongji Medical College, HUST.

2.3. *Preparation of DTC and FDT*

MC38 or CT26 cells were inoculated in 10 cm Petri dishes and cultured for 48 h to form a confluent monolayer. The complete medium was then replaced with 5 mL of blank medium, and cells were irradiated with different dosages of X-Ray. After 24 h, the cells were collected with a cell scraper and centrifuged at 1500 × *g* for 15 min (SL4 Plus, Thermo Fisher Scientific Co., Ltd., Shanghai, China) to precipitate the Dying Tumor Cells (DTC). Next, for preparation of Frozen Dying Tumor Cells (FDT), the obtained DTC were suspended in cell cryopreservation medium (80%DMEM, 20%FBS) at a cell density of 1×10^6 to 1×10^7/mL. The DTC suspension was then immediately immersed in liquid nitrogen for at least 12 h to obtain FDT-containing medium for preservation. The FDT-containing medium can be thawed at 37 °C and centrifuged at 1500 × *g* for 15 min to precipitate the Frozen Dying Tumor Cell (FDT). After washing with PBS twice, FDT was suspended in PBS and kept at 4 °C.

2.4. *SEM characterization of live cells, DTC, and FDT*

1×10^6 live cells, DTC, or FDT, were inoculated on a glass slide overnight. Then FDT were immobilized with 2.5% glutaraldehyde for 4 h, rinsed thrice with PBS, and dehydrated with gradient ethanol (30%, 50%, 70%, 80%, 90%, 95%, and 100%). Each gradient was processed once for 15 min, except for 100% ethanol, which was conducted twice to complete dehydration. Then, dehydrated cells were pictured by Nova NanoSEM 450 (Analytical and testing center of Huazhong University of Science and Technology, Wuhan, China).

2.5. *In vitro cell proliferation assay of DTC and FDT*

For *in vitro* cell proliferation, DTC and FDT prepared with different doses of X-ray radiation (10, 20, 40, 60, and 80 Gy) were suspended in a complete medium and added to 96-well plates with a density of 5×10^3 per well. After culturing for 0, 24, 48, 72 h, 10 μL of CCK-8 (Beyotime Biotechnology Shanghai, China) assay was added to each well. After incubation for 1 h, the absorbance was measured at 450 nm using a microplate reader.

2.6. *In vitro detection of apoptosis in FDT and DTC*

MC38 cells were cultured in 6 well-plates at a cell density of 2×10^5 cells per well for 24 h. Then, the complete medium was replaced with a blank medium, and cells were irradiated with the abovementioned X-ray dose to obtain DTC. After 24 h, DTC was collected and stained with Annexin V-FITC/PI double staining apoptosis detection kit (BestBio, Nanjing, China) according to the manufacturer's instructions for flow cytometry analyzation (BD Accuri C6, New Jersey, USA). For FDT, cells were resuspended in Annexin V buffer solution at a cell density of 1×10^6 cells/mL and stained with Annexin V-FITC/PI double staining apoptosis detection kit for flow cytometry analyzation.

2.7. *DNA damage assessment of DTC*

MC38 cells were treated with different dosages of irradiation (10, 20, 40, 60, and 80 Gy) as abovementioned. After 24 h, DTC were collected and lysed to extract proteins. The expression of γ-H2A.X in DTC was analyzed by western blotting analysis.

2.8. *Detection of intracellular dsDNA of FDT*

FDT and FC were treated with liquid nitrogen, frozen, and thaw cycle thrice, and centrifugated at $1500 \times g$ for 15 min to obtain supernatant containing cytoplasm content. Then, the intracellular dsDNA was quantified by NGS™ dsDNA HS Assay Kit (Wuhan ABP-Biosciences Co., Ltd., Wuhan, China) according to the manufacturer's instructions.

2.9. *In vitro maturation of BMDCs*

To obtain BMDCs, the C57BL/6 mice (female, 6 weeks old) were sacrificed to collect femurs and tibias. Then, bone marrow cells were separated and cultured with the complete RPMI-1640 medium containing GM-CSF (10 ng/mL) for 7 days to differentiate into BMDCs. On Day 7, LPS (1 μg per well), FC (50 μg protein per well), or FDT (50 μg protein per well) were added respectively. After incubating for 24 h, the cells were stained with APC-anti-CD11c, FITC-anti-CD80, PE-anti-CD86 and then detected by flow cytometry (BD Accuri C6) to quantify the percentage of matured DCs ($CD80^+$ $CD86^+$ in $CD11c^+$).

2.10. *In vitro polarization of BMDMs*

To obtain BMDCs, the C57BL/6 mice (female, 6 weeks old) were sacrificed to collect femurs and tibias. Then, bone marrow cells were separated and cultured with the complete DMEM medium containing M-CSF (20 ng/mL) for 5 days to differentiate into BMDMs. On Day 5, LPS (100 ng per well) + IFN γ (30 ng per well), FC (50 μg protein per well), FDT (50 μg protein per well), UNC2250 (5 μmol/L) or FDT (50 μg protein per well) + UNC2250 (5 μmol/L per well) were added respectively. After incubating for 24 h, the cells were harvested and stained with FITC-anti-F4/80, PE-anti-CD86, and APC-anti-CD206. The cells were then detected by flow cytometry (BD Accuri C6, USA) to quantify the percentage of M1 phenotype ($CD86^+$ in $F4/80^+$) and M2 phenotype ($CD206^+$ in $F4/80^+$) within BMDMs.

2.11. *In vitro M1-like polarization of Raw264.7 macrophages*

Raw264.7 macrophages were cultured in 12 well-plates at a cell density of 2×10^5 per well for 24 h. Then LPS (100 ng per well) + IFNγ (30 ng per well), FDT (50 μg protein per well), UNC2250 (5 μmol/L) or FDT (50 μg protein per well) + UNC2250 (5 μmol/L) were added. After incubating for 24 h, cells were collected and stained with PE-anti-F4/80 and FITC-anti-CD80. The samples were then detected by flow cytometry (BD Accuri C6) to quantify the percentage of M1-like macrophages ($CD80^+$ $F4/80^+$).

2.12. *In vitro internalization of FDT by macrophages and DCs*

Raw264.7 macrophages and DC2.4 were cultured in 12 well-plates at a cell density of 2×10^5 per well and cultured overnight. BMDMs were obtained and cultured in 24 well plates. The cells were then pretreated with blank DMEM medium or DMEM medium containing 25 μmol/L UNC2250 for 4 h. Next, DiD labeled FDT (FDT-DiD) was added. At 0.5, 1, and 2 h post-FDT co-incubation, the cells were harvested and analyzed by FCM (BD Accuri C6) to quantify the internalization of FDT by macrophages and DCs (DiD^+). For confocal laser scanning microscope (CLSM) observation, DC2.4 and Raw264.7 macrophages were seeded on the poly-L-lysine coated slides in 12-well plates and pretreated with blank DMEM or UNC2250 as mentioned above. After incubating with FDT-DiD for 2 h, the cells were labeled with tubulin tracker green staining and DAPI. Then, the internalization and location of FDT in DCs and macrophages were determined using CLSM (710META, Zeiss, Oberkochen, Germany).

2.13. *Characterization of the STING activation*

BMDCs, BMDMs, and Raw264.7 macrophages were stimulated, as previously mentioned. After incubating for 24 h, the cells were collected and lysed to extract proteins. The expression of STING and p-STING were analyzed by western blotting.

2.14. *Cytokine detection in the supernatant of DCs and macrophages*

BMDCs and BMDMs were stimulated, as previously mentioned. After incubating for 24 h, the cell-free supernatant was collected to quantify the concentration of pro-inflammatory cytokine (IFNβ, IL6, and TNFα) *via* a CBA cytokine kit.

2.15. *mRNA quantification of Ifnb1 in DCs and macrophages by qPCR*

BMDCs and BMDMs were stimulated, as previously mentioned. After incubating for 24 h, the cells were harvested to extract total RNA using Trizol (R1006, Beyotime Biotechnology, Shanghai, China). These extracted RNA were reverse transcribed to cDNA with hiscript ii reverse transcriptase. Then, the mRNA expression of *Ifnb1* was quantified with a quantitative polymerase chain

reaction with a real-time quantitative PCR instrument (Applied Biosystems Quantstudio™ 6&7, Thermo Fisher Scientific Co., Ltd., Shanghai, China). The qPCR primers used for the mRNA quantification of *Ifnb1* expression are m-*Ifnb1*-F: GGCTGTAT TCCCCTCCATCG, m-*Ifnb1*-R: CCATGTCCATGTAACAATG CCATGT.

2.16. *In vivo tumorigenicity assessment of DTC and FDT*

For *in vivo* tumorigenicity comparison, MC38 live cells were treated with 80 Gy radiation as the abovementioned preparation step to obtain DTC and FDT. Then, female C57BL/6 mice were randomly divided into five groups, including live cells, DTC-1 $\times$ 10^6, DTC-5 $\times$ 10^6, FDT-1 $\times$ 10^6, FDT-5 $\times$ 10^6. For the live cells group, mice were intraperitoneally transplanted with 1 $\times$ 10^6 live MC38 cells On Day 0. For DTC and FDT groups, mice were intraperitoneally injected with 1 $\times$ 10^6/5 $\times$ 10^6 DTC or FDT on Days 0, 4, and 8. On Day 25, mice were sacrificed, and tumor tissue was harvested and weighted to measure the tumorigenicity of DTC and FDT.

2.17. *Prophylactic vaccination of FDT on subcutaneous tumor*

The female C57BL/6 mouse was randomly divided into seven groups, including PBS, FC, FDT-10 Gy, FDT-20 Gy, FDT-40 Gy, FDT-60 Gy, FDT-80 Gy, and treated with subcutaneous injection of PBS, FC (1 $\times$ 10^6 cell per mouse), FDT (1 $\times$ 10^6 cell per mouse) on the right flank on Day -14, and -7. On Day 0, 2.5 $\times$ 10^5 MC38 cells were then inoculated into the left flank of mice. The tumor size and body weight were monitored every two days. Except for natural death, mice were considered dead and euthanized when tumor volume grew larger than 1500 mm^3. The survival rate was monitored and recorded until the 90th day post-tumor inoculation.

2.18. *Therapeutic vaccination of FDT on peritoneal carcinomatosis of MC38 and CT26*

To establish a peritoneal carcinomatosis model, female C57BL/6 mice were intraperitoneally transplanted with 5 $\times$ 10^5 MC38 cells. And female BALB/c mice were intraperitoneally transplanted with 5 $\times$ 10^5 CT26 cells. MC38 tumor-bearing mice were divided into five groups, recorded as PBS, FC, FDT-40 Gy, FDT-60 Gy, and FDT-80 Gy CT26 tumor-bearing mice were randomly divided into eight groups, recorded as PBS, oxaliplatin, FC, FDT-10 Gy, FDT-20 Gy, FDT-40 Gy, FDT-60 Gy, FDT-80 Gy). On Days 3, 7, and 11, mice in different groups were intraperitoneally injected with PBS, oxaliplatin (6 mg/kg), FC (1 $\times$ 10^6 cells per mouse), and FDT (1 $\times$ 10^6 cells per mouse). Finally, MC38 tumor-bearing mice were sacrificed on Day 20, and CT26 tumor-bearing mice were sacrificed on Day 16. The tumor nodules in the peritoneal cavity were harvested and weighed. Ascitic fluid was aspirated entirely directly from the peritoneal cavity for volume measurement.

2.19. *Examination of the therapeutic efficiency of FDT combined with UNC2250*

Mice with MC38 peritoneal tumors were randomly divided into five groups and treated with an intraperitoneal injection of PBS, oxaliplatin (6 mg/kg), FDT (1 $\times$ 10^6 cells per mouse), UNC2250 (25 mg/kg) or FDT + UNC2250 (1 $\times$ 10^6 cells per mouse+25 mg/kg) on Days 3, 7, and 11. The tumor-bearing mice were sacrificed on Day 22. The tumor nodules in the peritoneal cavity were harvested and weighed. Ascitic fluid was aspirated entirely directly from the peritoneal cavity for volume measurement. Similarly, mice with CT26 peritoneal tumor were treated as described before. And mice were sacrificed on Day 16. The tumor nodules in the peritoneal cavity and peritoneum were harvested and weighed. Ascitic fluid was aspirated entirely directly from the peritoneal cavity for volume measurement.

2.20. *Flow cytometry analysis of tumor-associated immune cells*

For flow cytometry analysis, harvested tumors were minced into small pieces with scissors and incubated in a digestion buffer at 37 °C for 70 min. The suspensions were filtrated using a cell strainer (BD Falcon, New Jersey, USA) and centrifuged at 2000 rpm for 5 min. The collected cells were re-suspended in ACK Lysis Buffer to remove red blood cells. Next, the obtained cells were resuspended in PBS and stained by Fixable Viability Dye eFluor™ 780 (Thermo Fisher Scientific Co., Ltd., Shanghai, China) to exclude dead cells. Then, cells were washed with PBS and stained with anti-CD16/CD32 antibody (BD, New Jersey, USA) for Fc blocking to prevent nonspecific binding. Subsequently the cells were incubated with Percp-Cy5.5-anti-CD45, BV510-anti-CD3, FITC-anti-CD4, BV421-anti-CD8, PE-anti-B220, APC-anti-CD11c, FITC-anti-CD11b, PE-anti-F4/80, BV650-anti-CD86 and PE-Cy7-anti-CD206 (BD, Shanghai, China) to specifically label the T lymphocytes, B lymphocytes, DCs and Macrophage. Expect Fixable Viability Dye eFluor™ 780 and anti-CD16/32. All the above staining and centrifugation processes were carried out at 4 °C under darkness. The samples were analyzed by FCM (Sony ID7000™, Tokyo Metropolis, Japan).

2.21. *Statistical analysis*

All data analyses were conducted using GraphPad Prism 8.0 software. All results are presented as mean $\pm$ standard deviation (SD). For two groups, the two-tailed Student's *t*-test was used for statistical analysis. For multiple groups (three or more groups), one-way analysis of variance (ANOVA) was used for statistical analysis, followed by Tukey's multiple comparisons test as post-hoc analysis. Statistical significance was present as $^{*}P < 0.05$, $^{**}P < 0.01$, and $^{***}P < 0.001$.

3. Result

3.1. *High immunogenic FDT vaccine for multiple colon cancer*

During vaccine preparation, X-ray radiation is a vital step to induce the ICD of tumor cells. The radiation dose may directly impact the therapeutic efficiency of FDT. However, the dose-response relationship between the immunogenicity of cancer cells and X radiation dose remained unexplored. Thereby, we designed a dose gradient in the procedure of X radiation-based vaccine preparation, including five radiation doses (10, 20, 40, 60, and 80 Gy) (Fig. 1A). The immunogenicity and therapeutic efficiency of these FDT vaccines prepared under different radiation doses were evaluated both *in vitro* and *in vivo*.

Recently, growing evidence has supported that a DNA damage response can enhance immunogenicity by activating cytosolic

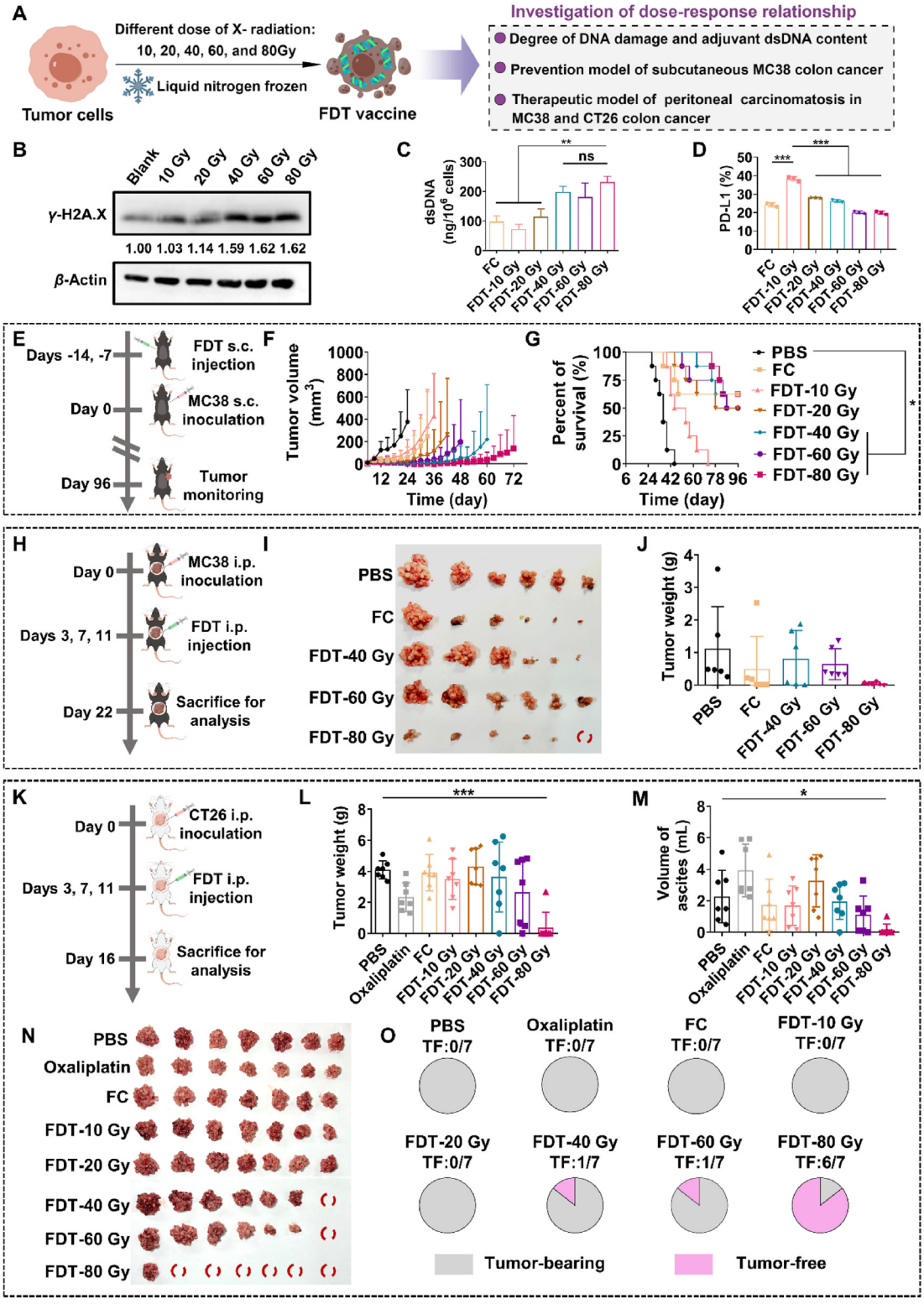

Figure 1 The immunogenicity of the FDT vaccine was positively correlated with radiation dose. (A) Schematic illustration of the investigation in the dose-response relationship between cancer cells' immunogenicity and X-ray dose. (B) The expression of γ-H2A.X in DTC induced by different radiation doses. (C) Quantification of intracellular dsDNA in FDT prepared with different radiation doses ($n = 4$). (D) Expression of PD-L1 in FDT prepared with different radiation doses ($n = 3$). (E) Schematic illustration of prophylactic FDT vaccination and subsequent challenge with subcutaneous MC38 tumor model. (F) The average tumor growth curve and (G) survival rate curve of mice in different groups ($n = 8$). (H) Schematic illustration of therapeutic FDT vaccination for MC38 peritoneal carcinomatosis. (I) Tumor images and (J) average tumor weight of MC38 peritoneal carcinomatosis in different groups ($n = 6$). (K) Schematic illustration of therapeutic FDT vaccination for CT26 peritoneal carcinomatosis. (L) Tumor images, (M) average tumor weight, (N) average ascites volume, and (O) tumor-free rate of CT26 peritoneal carcinomatosis in different groups ($n = 7$). Note: the red circle represents tumor-free. Diagrammatic drawings in (A), (D), (G), and (J) were created by Figdraw. Data are presented as mean ± SD. $^*P < 0.05$, $^{**}P < 0.01$, $^{***}P < 0.001$; ns, not significant.

immunity and ICD[18]. During ICD, several essential DAMP signals, like calreticulin (CRT), ATP, high mobility group box 1 (HMGB1), and annexin A1 (ANXA1), are activated following DNA damage in tumor cells[19]. Besides, DNA damage can trigger an excessive accumulation of double-stranded DNA (dsDNA) fragments in the cytoplasm, which is a potent adjuvant to activate type I interferon response within the tumor. Since X-radiation has been demonstrated to trigger a potent intracellular DNA damage effect, we first measured the DNA damage level by Western blot (WB). The expression of γ-H2A.X in the DTC of MC38 cells, which is a sensitive molecular marker of DNA damage, exhibited a marked increase after 40 Gy, 60 Gy, and 80 Gy radiation treatments compared with that of 10 Gy, and 20 Gy radiation treatments (Fig. 1B). Consistently, the dsDNA quantification by NGS™ dsDNA HS Assay Kit also revealed that the dsDNA content in FDT prepared by 40 Gy, 60 Gy, and 80 Gy also vastly increased (Fig. 1C). In addition to the enhancement of immunostimulatory signaling, X-Ray can also promote the expression of programmed cell death protein-ligand 1 (PD-L1) on FDT, which can bind to the programmed cell death protein-1 (PD-1) on T lymphocytes, thus suppressing the antitumor efficiency. Interestingly, we found that only X-radiation in 10 Gy led to a significantly higher expression of PD-L1 on FDT (Fig. 1D), indicating stronger immunosuppression during vaccination. The above observations demonstrated that a relatively higher radiation dose may be beneficial to induce more robust immunogenicity in the FDT vaccine.

However, given that the tumor microenvironment (TME) is highly immunosuppressive and irreversible for most of strategy[20-22], it remained an open question whether the immunogenicity of the FDT vaccine was sufficient to elicit an effective antitumor response *in vivo*. Therefore, we examined the FDT-induced protective immunity against the challenge of live MC38 cells in immunocompetent mice, which has been widely accepted as the primary standard to examine the immunogenicity of cancer vaccine[23-25]. In our design, mice were subcutaneously vaccinated with FDT on the right flank twice. One week after the latest vaccination, mice were challenged with live MC38 cells on the left flank, and the subsequent tumor progression was monitored for 75 days (Fig. 1E). Meanwhile, frozen cells (FC) without X-irradiation were utilized as control. The results revealed that the FDT vaccine prepared by different radiation dosages showed a certain inhibitory effect on tumorigenesis and tumor growth (Fig. 1F and G, Supporting Information Fig. S1A). Significantly, in mice vaccinated with FDT-40 Gy, FDT-60 Gy, and FDT-80 Gy, the onset of tumor growth was largely delayed compared with other vaccinated groups. Most importantly, this FDT vaccination maintained evidently higher survival rates (≥4/8) over 98 days.

To figure out the optimal radiation dose, the therapeutic efficiency of FDT-40 Gy, FDT-60 Gy, and FDT-80 Gy was further investigated in a more challenging peritoneal carcinomatosis of MC38 colon cancer. Mice were inoculated with MC38 cells into the peritoneal cavity. On Days 3, 7, and 11 post-tumor inoculations, mice were vaccinated with FDT into the peritoneal cavity. On Day 22, post-tumor inoculation, mice were sacrificed, and tumor nodules were harvested and weighed (Fig. 1H). Notably, FDT-80 Gy inhibited tumor growth by 95.8% dramatically and implemented complete tumor regression of peritoneal tumors (tumor-free) in 1/6 mice, which is much more effective than the other groups (Fig. 1I and J). More importantly, the infiltration of DCs primarily increased within the tumor (Fig. S1B). Consistently, $CD4^+$ and $CD8^+$T lymphocytes also increased significantly after FDT-80 Gy treatment, indicating an effective T lymphocyte immunity cell response within the tumor (Fig. S1C). Thus, it can be seen that FDT-80 Gy possessed much higher efficiency in tumor inhibition and immune activation for treating MC38 peritoneal carcinomatosis.

Next, to verify the universality of this vaccine system, we further examined the effectiveness of FDT in the peritoneal carcinomatosis of CT26. Compared with MC38, CT26 metastasizes more rapidly and is accompanied by severe ascites at advanced stage. More intractably, CT26 is an MSS-type colon cancer cell line with the typical manifestation of exiguous immune cell infiltration and poor prognosis in response to immunotherapy[26]. In our experimental design, CT26 tumor-bearing mice were intraperitoneally vaccinated with FDT, prepared under the abovementioned radiation doses on Days 3, 7, and 11 post-tumor inoculations, and sacrificed on Day 16 (Fig. 1K). Besides, the first line of chemotherapeutics drug, oxaliplatin, was applied as the positive control for the treatment of colon cancer. Unexpectedly, oxaliplatin showed undesirable tumor inhibition and malignant ascites regression for MSS tumor (Fig. 1L and M). In contrast, FDT-80 Gy treatment exhibited the strongest tumor inhibition and malignant ascites regression in this immunosuppressive cold tumor (Fig. 1L–O), which was consistent with previous observations in the PCCC model of MC38. More importantly, 6/7 of mice in the FDT-80 Gy group achieved complete elimination of tumor and malignant ascites. The average volume of malignant ascites in FDT-80 Gy groups decreased by 94% compared with the PBS group. The neovascularization on the surface of the peritoneum was obviously fewer (Fig. S1D). This was again verified in intratumor vascular staining results, in which $CD31^+$ blood vessels were largely reduced in FDT-80 Gy groups (Fig. S1E).

The above results revealed that the immunogenicity and antitumor efficiency of FDT vaccines were positively correlated with the radiation dose. In particular, FDT prepared with 80 Gy X-radiation showed significantly enhanced therapeutic efficiency in the peritoneal carcinomatosis model of CT26 and MC38 colon cancer. Even in the immunosuppressive peritoneal carcinomatosis model of CT26, FDT-80 Gy treatment was far more effective than oxaliplatin treatment.

3.2. *FDT is a safe vaccine ingredient with high-efficiency*

Having optimized the dose of X-ray for FDT preparation, we started to investigate the morphology and safety of FDT and further investigated the appropriate mode of administration for FDT vaccination. During vaccine preparation, X-irradiation and freezing techniques were introduced to enhance the immunogenicity and safety of vaccines, respectively. The process was characterized and verified by scanning electron microscopy (SEM) and flow analysis. Under SEM observation, both DTC and FDT maintained the integrity of cell morphology (Fig. 2A). Flow cytometry analysis revealed that the side scatter (SSC) values of DTC and FDT were similar to those of live cells, indicating the reservation of internal structure and cellular content (Fig. 2B). And the reduction of forward scatter (FSC) value in FDT meant the shrinkage of cellular size. The above results demonstrated that the FDT vaccine maintained the integrity of tumor cells.

Since FDT and DTC originated from live tumor cells, they may still retain the tumorigenicity from cancer cells, which was a potential safety hazard. It was highly necessary to investigate the tumorigenicity of FDT and DTC. At 24 h post-irradiation, about

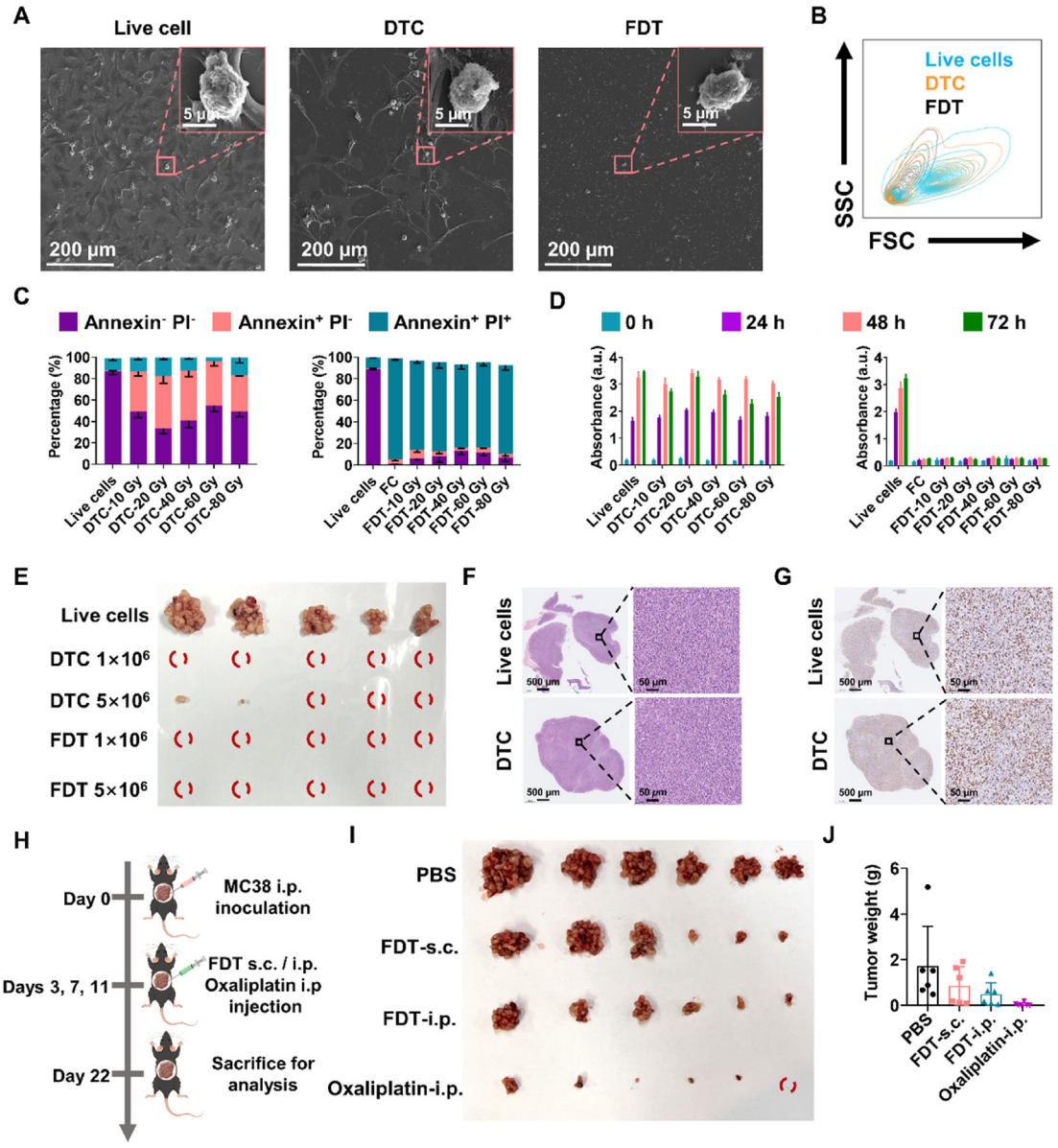

Figure 2 FDT is a safe vaccine ingredient with high efficiency. (A) SEM images of live tumor cells, DTC, and FDT (scale bar = 200 μm and 5 μm). (B) FCM analysis of live cells, DTC, and FDT. (C) The percentages of non-apoptotic cells (Annexin$^-$ PI$^-$), early apoptotic cells (Annexin$^+$ PI$^-$), and late apoptotic cells (Annexin$^+$ PI$^+$) in DTC and FDT at 24 h post-X-Ray (n = 3). (D) *In vitro* proliferation ability analysis of live cells, DTC, and FDT by CCK8 (n = 6). (E) Image of *in vivo* tumorigenesis after i.p. injection of FDT or DTC thrice (n = 5). (F) IHC images of HE and (G) Ki67 staining of peritoneal MC38 tumor excised from mice after i.p. injection of live cells and DTC (scale bar = 500 and 50 μm). (H) Schematic illustration of different modes of administration for FDT vaccination in MC38 peritoneal carcinomatosis. (I) Tumor images and (J) average tumor weights of peritoneal carcinomatosis in different groups (n = 6). Note: the red circle represents tumor-free. Diagrammatic drawing in (H) was created by Figdraw. Data are presented as mean ± SD.

50% of DTC were alive (Annexin V$^-$ PI$^-$) and the portion of late-stage apoptotic cells (Annexin V$^+$ PI$^+$) in DTC was only 10%−20% (Fig. 2C). After liquid nitrogen frozen and thawing treatment, the percentage of non-viable apoptotic cells in FDT and FC (unirradiated tumor cells treated with liquid nitrogen frozen technique) was upregulated to 80%−90%. Next, we examined the *in vitro* proliferation activity of live cells, DTC, FC, and FDT by CCK8 assay (Fig. 2D). The results suggested that DTC can proliferate rapidly, just like live tumor cells, within 72 h. Different from DTC, the proliferation of FDT and FC in 72 h remained unchanged, indicating that liquid nitrogen frozen treatment can largely dispel the intrinsic proliferation activity of tumor cells. Subsequently, we compared the proliferation activity of DTC and FDT *in vivo*. Consistent with *in vitro* proliferation, three times intraperitoneal injection of FDT (at the doses of 1×10^6 and 5×10^6 cells per mouse) did not lead to tumorigenesis *in vivo* (Fig. 2E−G). In contrast, DTC can quickly proliferate *in vivo* and cause tumorigenesis when the administration dose reaches 5×10^6 cells per mouse. Meanwhile, the body weight and the routine blood results of FDT-injected mice remained in a

reasonable fluctuation, indicating the excellent biosafety of FDT (Supporting Information Fig. S2). Combined with *in vitro* and *in vivo* proliferation assays, FDT was as reliable as cancer vaccines due to its elimination of tumorigenicity and few side effects.

Next, we examined the dose-responsive relationship between the dosage of FDT administration and therapeutic efficiency on peritoneal carcinomatosis of MC38 colon cancer. Meanwhile, we utilized conventional agents (oxaliplatin and irinotecan) as the positive control. The results revealed that a relatively low dose (1×10^6 FDT per mouse) for FDT administration was enough to achieve effective tumor inhibition, which could outperform irinotecan (Supporting Information Fig. S3). Furthermore, we speculated whether there is a more effective mode of administration compared with i.p. injection. Our previous research proved that subcutaneously injected whole-cell vaccine or extracellular vesicle (EV) can drain into lymph nodes (LNs), thus activating anticancer immunity[9,27,28]. Hence, we compared the therapeutic efficiency of FDT through intraperitoneal and subcutaneous injection (Fig. 2H). However, intraperitoneal injection of FDT was still more effective in inhibiting tumor growth than subcutaneous injection of FDT (Fig. 2I and J). Accordingly, i.p. injection might be the most suitable method for FDT vaccination to exert 100% therapeutic efficiency in peritoneal carcinomatosis of colon cancer.

3.3. *FDT showed completely different immune activation effects on DCs and macrophages*

In the previous observation, FDT demonstrated potent tumor inhibition in CT26 and MC38 models of peritoneal carcinomatosis. Inspired by this, we next explored the mechanism of FDT-induced antitumor immunity by analyzing the subtypes of different immune cells in TME. In our experiment designs, the CT26 tumor-bearing mice were treated with PBS, FDT, or oxaliplatin on Days 3, 7, and 11 and sacrificed on Day 16. The tumor tissues were then harvested for immune mechanism analysis (Fig. 3A). As expected, FDT promoted intra-tumoral infiltration of both helper T lymphocytes ($CD3^+$ $CD4^+$ $CD45^+$) and cytotoxic T lymphocytes ($CD3^+$ $CD8^+$ $CD45^+$) (Fig. 3B and C; Supporting Information Fig. S4A and S4B). Significantly, the portion of $CD3^+$ $CD4^+$ T lymphocytes in FDT groups was 6.82-fold higher than that of the oxaliplatin-treated group. Besides the effective priming of cellular immunity, FDT could also trigger the infiltration of a large number of B lymphocytes ($B220^+$ $CD45^+$) into TME effectively (Fig. 3D; Fig. S4C), whereas B cells barely existed in PBS and oxaliplatin groups, indicating a robust humoral immunity induced by FDT in TME. Overall, the above results suggested that FDT could trigger potent adaptive immunity for tumor inhibition.

For the initiation and regulation of adaptive immunity, antigen presentation cells (APCs), including DCs and macrophages, play a crucial role[29,30]. Upon taking up tumor-associated antigens (TAAs) in the vaccine, quiescent APCs transformed into the activated state to transmit TAAs to T lymphocytes, eliciting tumor-specific cytotoxic T cells to eliminate cancer cells[30]. Indeed, FDT can activate DCs more effectively compared with oxaliplatin, manifesting as a significantly higher portion of mature DCs ($CD86^+$ in $CD11c^+$) in the FDT group (Fig. 3E; Fig. S4D). Additionally, the $CD8\alpha^+$ DCs subsets, which can specifically transmit TAAs to cytotoxicity T lymphocytes, exhibited a 3.2-fold up-regulation in the FDT group compared with that of the oxaliplatin group (Fig. 3F; Fig. S4E). Despite FDT effectively resulting in the potent maturation of DCs within TME, the M1-like polarization of macrophage barely increased in response to FDT vaccination (Fig. 3G; Fig. S4F). We proposed that FDT may have a different efficiency in activating DCs and macrophages. To figure out this unique phenomenon, we examined the *in vitro* immune activation status and signal channel changes of bone-marrow-derived dendritic cells (BMDCs) and bone marrow-derived macrophage (BMDMs) in response to FDT stimulation (Fig. 3H). With the stimulation of FDT, the portion of mature BMDCs ($CD86^+$ $CD80^+$ in $CD11c^+$) was dramatically upregulated to 70%, which was comparable to the treatment of lipopolysaccharide (LPS) served as the positive control (Fig. 3I). But for BMDMs, the portion of M1-phenotype macrophage ($CD86^+$ in $F4/80^+$) in FDT group remained at the same level as the blank control group, indicating that FDT was ineffective at M1-like polarization of macrophages (Fig. 3J). These results indicated that FDT showed contrary immune activation efficiency on DCs and macrophages *in vivo* and *in vitro*.

Having demonstrated that FDT can only induce immune activation in DCs rather than macrophages, we next investigated the underlying mechanism. Given that the highly abundant dsDNA accumulated in FDT might induce type I interferon response in APCs, thereby actively regulating various physiological processes, including maturation, antigen presentation, and cross-priming of cytotoxic T cells[13,17,31], we next examined the type I interferon response of DCs in response to the stimulation of FDT. Indeed, FDT largely upregulated the mRNA expression of *Ifnb1* in BMDCs and finally boosted the IFNβ production by 2-fold compared with the FC group (Fig. 3K and L), validating robust type I interferon response induced by FDT stimulation. Entirely contrary, the mRNA expression of *Ifnb1* and the cytokine secretion of IFNβ in macrophages just exhibited an unnoticeable enhancement with FDT treatment (Fig. 3M and N). This observation demonstrated that the FDT-induced type I interferon response was restricted to DCs, consistent with our findings that FDT can only induce the maturation of DCs rather than the M1-like polarization of macrophages. Furthermore, growing evidence proved that the STING signal is the key mechanism that drives the antitumor type I interferon response. Thus, we detected the activation status of the STING pathway in DCs and macrophages, which served as sensing signaling of dsDNA for the induction of type I interferon response. As shown in Fig. 3O, with the stimulation of FDT, the expression of phospho-STING (p-STING) in BMDCs increased significantly compared with FC and LPS treatment. However, for macrophages, FDT only demonstrated an unnoticeable augmentation of the p-STING expression compared with FC treatment (Fig. 3P). The above results illustrated that FDT could activate the STING pathway in DCs, thus triggering a robust type I interferon response and subsequent maturation of DCs. In contrast, it failed to elicit type I interferon response and M1-like polarization in macrophages *via* the STING signaling pathway.

In summary, FDT exhibited a completely contrasting effect on macrophages and DCs, which can only activate DCs rather than macrophages. The failure in the immune activation of macrophages may be related to the inability of dsDNA in FDT to activate STING and induce type I interferon response. Given that macrophages are the most abundant immune cells in TME and play a central role in innate immunity[17], more advanced FDT vaccination strategies should be developed to enhance M1-like macrophage polarization and incorporate two branches of adaptive and innate antitumor immunity.

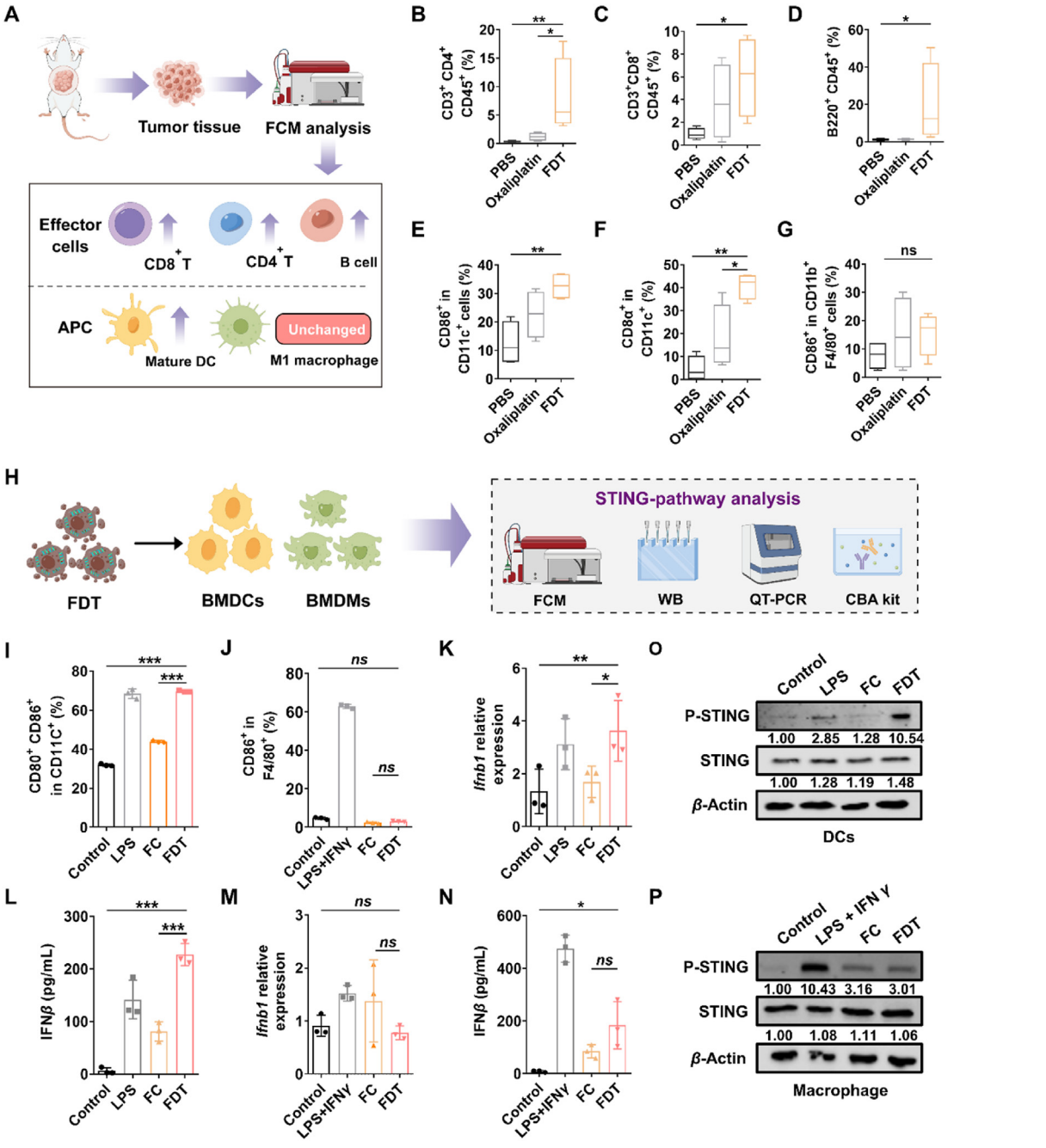

Figure 3 FDT showed completely different immune activation effects on DCs and macrophages. (A) Schematic illustration of immune subtype analysis in CT26 peritoneal tumor. (B) $CD4^+$ T lymphocytes ($CD3^+$ $CD4^+$ $CD45^+$), (C) $CD8^+$ T lymphocytes ($CD3^+$ $CD8^+$ $CD45^+$), (D) The percentage of B cells ($B220^+$ $CD45^+$), (E) matured DCs ($CD86^+$ in $CD11c^+$), (F) $CD8\alpha^+$ DCs ($CD8\alpha^+$ in $CD11c^+$) and (G) M1-like macrophages ($CD86^+$ in $CD11b^+$ $F4/80^+$) within tumor ($n = 4$). (H) The schematic illustration of the STING-pathway analysis in BMDCs and BMDMs by flow cytometry, qPCR, CBA, and Western blot. (I) The percentage of maturation in BMDCs ($CD80^+$ $CD86^+$ in $CD11c^+$) and (J) the percentage of M1 phenotype BMDMs ($CD86^+$ in $F4/80^+$) ($n = 3$). (K) The mRNA expression of *Ifnb1* and (L) the secretion of IFNβ in BMDCs after different treatments ($n = 3$). (M) The mRNA expression of *Ifnb1* and (N) the secretion of IFNβ in BMDMs after different treatments ($n = 3$). (O, P) The expression of P-STING and STING in BMDCs and Raw264.7 macrophages after different treatments. Diagrammatic drawings in (A) and (H) were created by Figdraw. Data are presented as mean ± SD. $^*P < 0.05$, $^{**}P < 0.01$, $^{***}P < 0.001$; ns, not significant.

3.4. UNC2250 inhibited the efferocytosis of macrophages on FDT to restore the immune activation effect on macrophages

The current FDT vaccine strategy just showed limited efficacy in promoting STING activation and anti-tumorigenic M1-like polarization of macrophages. Therefore, we next explored the underlying mechanism of the immunologically silent state in macrophages with FDT stimulation.

Recent research has found that the massive exposure of PS on apoptotic cells can result in efferocytosis of macrophages and

achieve immunosuppressive clearance of apoptotic cells in TME[32,33]. During this process, MerTK is an important phagocytic receptor on macrophages, which directly mediates the identification of apoptotic cells[15,34]. Therefore, we speculated that in TME, MerTK on TAMs may recognize and bond with PS exposed on apoptotic FDT to facilitate the rapid removal of TAAs and DAMPs signal before alerting the innate immune system (Fig. 4A). Notably, the detection of PS exposure on the surface of FDT revealed that X-radiation and liquid nitrogen frozen process will result in massive PS exposure on the surface of FDT compared with live cells (Fig. 4B). Thus, FDT will be largely engulfed and cleared by macrophages. Upon pretreated with MerTK inhibitor UNC2250 (at least 4 h early), macrophages, including BMDMs and Raw264.7 cell lines, showed substantially reduced phagocytosis of FDT with an inhibitory rate of 59.6% and 80% in 2 h, respectively (Fig. 4C and D; Supporting Information Fig. S5A−S5D), validating that the inhibition of the interaction between MerTK and PS could effectively inhibit the clearance of FDT by macrophages. In contrast, DCs pretreated with UNC2250 showed almost unchanged uptake capacity of FDT (Fig. 4C), indicating that DCs can still uptake FDT even in the presence of UNC2250 and may retain favorable immune activation effects.

Moreover, with the effective blockade of macrophage-mediated clearance by UNC2250, FDT showed significantly enhanced STING activation in macrophages. In BMDMs, the combinational stimulation of FDT and UNC2250 largely upregulated the phosphorylation of STING (Fig. 4E). Correlated with the effective STING activation, the combinational strategy boosted the mRNA expression of *Ifnb1* by 3.77-fold compared with FDT treatment, thus triggering a massive secretion of IFNβ, which was 2.67-fold higher than that of FDT group (Fig. 4F and G). Besides, the secretion of other pro-inflammatory cytokines, including IL6 and TNFα, also largely increased (Fig. 4H and I). With the potent activation of the STING pathway in macrophages, we examined whether this combinational strategy could also induce a robust M1-like polarization of macrophages. As shown in Fig. 4J−L, the percentage of M1 phenotype BMDMs ($CD86^+$ in $F4/80^+$) was rapidly upregulated in combinational groups by 3-fold compared with control groups. The M1/M2 ratio in the combinational group was 13.6-fold higher than the FDT group (Fig. 4L). A similar result was observed in Raw264.7 cell lines (Fig. S5E). The underlying mechanism of these results may largely be attributed to the increasing release of cGAMP and dsDNA from FDT after MerTK inhibition, thereby entering macrophages to activate the STING pathway and M1-like polarization[16]. Therefore, combining FDT with UNC2250 may be an advantageous synergistic strategy to facilitate the simultaneous activation of DCs and TAMs.

3.5. *UNC2250 synergistically enhanced antitumor efficiency of FDT vaccine*

Encouraged by the findings that combining UNC2250 with the FDT vaccine could exert significantly enhanced M1-like polarization and STING activation of macrophage *in vitro*, we examined the therapeutic efficiency of this combinational strategy *in vivo* on MC38 model (Fig. 5A). For the treatment of MC38 peritoneal carcinomatosis, UNC2250 monotherapy can barely inhibit tumor progression. Although FDT has already demonstrated excellent antitumor efficacy, the combinational treatment of FDT and UNC2250 resulted in a substantial 79% reduction in average tumor weight compared with FDT alone (Fig. 5B and C). Meanwhile, it is worth noting that 2/6 mice in the FDT + UNC2250 combination group were tumor-free, which overmatched oxaliplatin treatment. In addition, the immunofluorescence (IF) results revealed that the amount of $F4/80^+$ (biomarker of macrophages) cells in the combinational group was higher compared with that in the FDT group (Supporting Information Fig. S6), indicating increased infiltration of macrophages in TME. Moreover, there was a higher expression level of i-NOS (the biomarker of M1 macrophages) in the combinational group (Fig. 5D). And consistent with the *in vitro* efferocytosis inhibition results, the distribution of cleaved-$caspase3^+$ cells in the combinational group significantly increased compared with other groups, indicating the massive accumulation of apoptotic cells within the tumor (Fig. 5E).

For the immunosuppressive CT26 model, the combinational strategy also exhibited the strongest inhibition of tumor burden and malignant ascites (Fig. 5F−J). Compared with FDT monotherapy, the combinational treatment further reduced tumor weight by 87% (Fig. 5H). More importantly, the combinational treatment resulted in a complete regression of ascites in all mice (Fig. 5I) and tumor-free in 5/8 mice (Fig. 5J). In addition, the MerTK expression in tumors was significantly reduced after UNC2250 treatment (Supporting Information Fig. S7). Consistently, IHC images revealed that combinational treatment resulted in large areas of apoptosis within the tumor, which was not observed in other groups (Supporting Information Fig. S8). Overall, these results demonstrated that the combinational treatment of FDT + UNC2250 can primarily enhance the antitumor efficiency of the FDT vaccine. Given that PCCC is still intractable for the current clinical strategy, this combinational vaccine strategy may provide a potential therapeutic regimen.

3.6. *The combination of FDT and UNC2250 facilitated the double activation of adaptive and innate immunity*

Given the outstanding tumor inhibition rate and the M1-like polarization of this combination therapy (FDT + UNC2250), we next explored *in vivo* immune activation effects of this combinational treatment on peritoneal tumors (Fig. 6A). The CT26 tumor-bearing mice were treated as described previously, and sacrificed on Day 16 to obtain tumor tissue and spleen for immune analysis (Supporting Information Figs. S12−S14). In tumor, the combinational treatment significantly raised the M1-like polarization of TAMs ($CD86^+$ in $F4/80^+$ $CD11b^+$) by 2-fold compared with FDT mono-treatment (Fig. 6B). Meanwhile, the M2-like polarization of TAMs was also significantly restrained (Fig. 6C). Besides the effective M1-like polarization of TAMs, the portion of mature DCs ($CD86^+$ in $CD11c^+$) in TME was also upregulated by 1.5-fold compared with FDT groups (Fig. 6D), which may be attributed to the effective blockade of efferocytosis. Consistent with the cooperative activation of adaptive immunity and innate immunity after the combinational treatment, the production of TNFα within the tumor significantly increased compared with the mono treatment of FDT (Supporting Information Fig. S9). Moreover, the combinational treatment resulted in increasing expression of IgG and IgM within the tumor (Fig. 6E; Supporting Information Fig. S10), which are the major antibodies secreted by effector B lymphocytes to elicit antibody-dependent cell-mediated cytotoxicity (ADCC) and complement-dependent cytotoxicity (CDC) against tumor respectively[35-37].

In the spleen, the portion of M1 phenotype macrophages also largely increased by 5-fold compared with the PBS group (Fig. 6F; Supporting Information Fig. S11A), indicating the

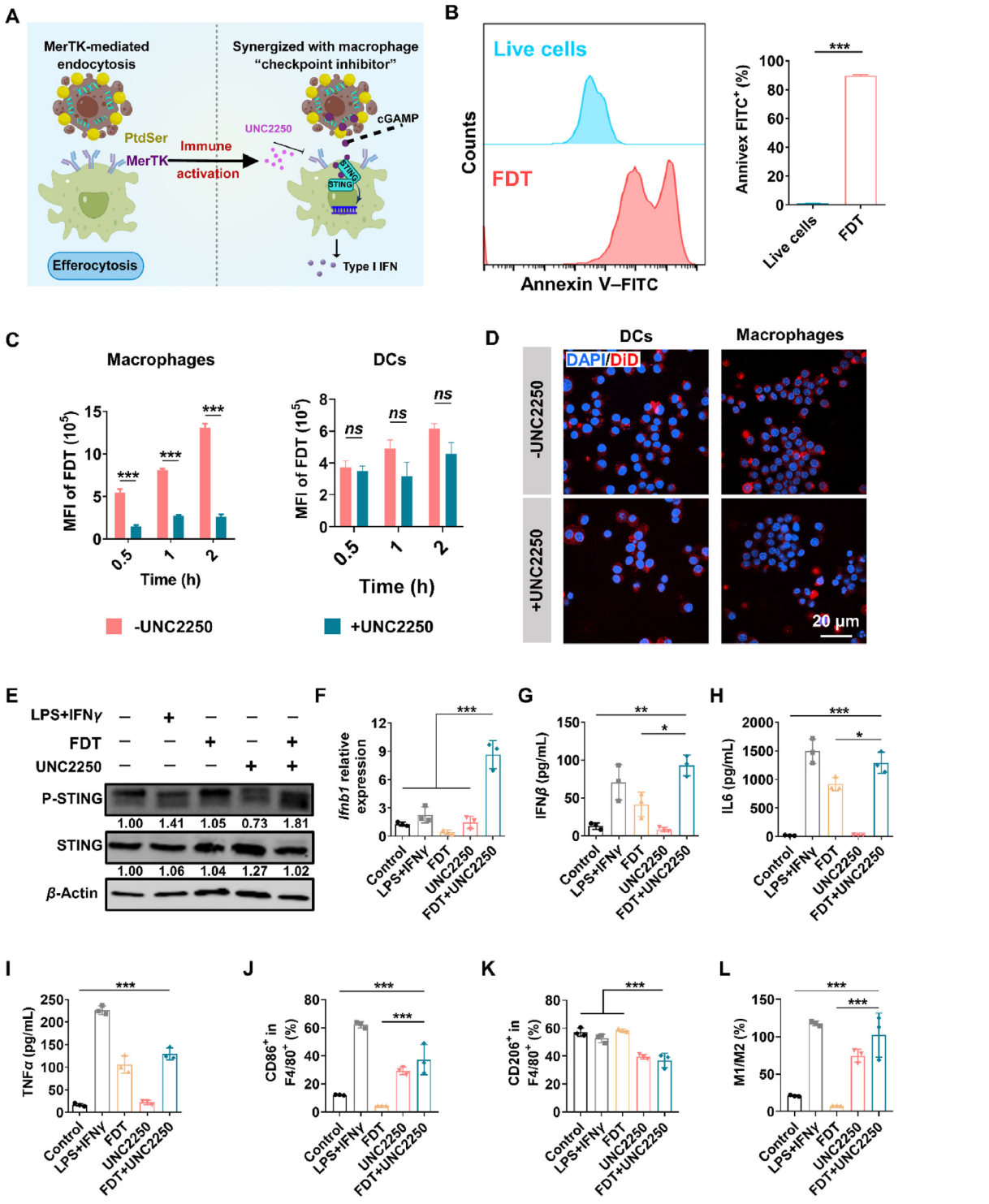

Figure 4 UNC2250 precluded the immunosuppressive clearance of FDT by macrophages to restore the immune activation effect on macrophages. (A) Schematic illustration of UNC2250-induced efferocytosis inhibition on macrophages and subsequent immune activation. (B) Representative flow cytometry plots and quantitative analysis of phosphatidylserine (PS) exposed on FDT and live cells *via* Annexin V−FITC dyeing ($n = 3$). (C) The quantitative analysis of UNC2250 induced different inhibition efficiency on FDT uptake by macrophages and DCs *in vitro* ($n = 3$). (D) Representative CLSM images of Raw264.7 macrophages and DC2.4 internalization to FDT for 4 h with or without UNC2250 pretreatment (scale bar = 20 μm). (E) The expression levels of P-STING and STING in BMDMs after different treatments. (F) The mRNA expression level of *Ifnb1* and (G−I) the secretion of IFNβ, IL6, and TNFα in BMDMs after different treatments ($n = 3$). (J) The percentages of M1 phenotype, (K) M2 phenotype, and (L) the ratio of M1/M2 in BMDMs with different treatments ($n = 3$). The diagrammatic drawing in (A) was created by Figdraw. Data are presented as mean ± SD. $^*P < 0.05$, $^{**}P < 0.01$, $^{***}P < 0.001$; ns, not significant.

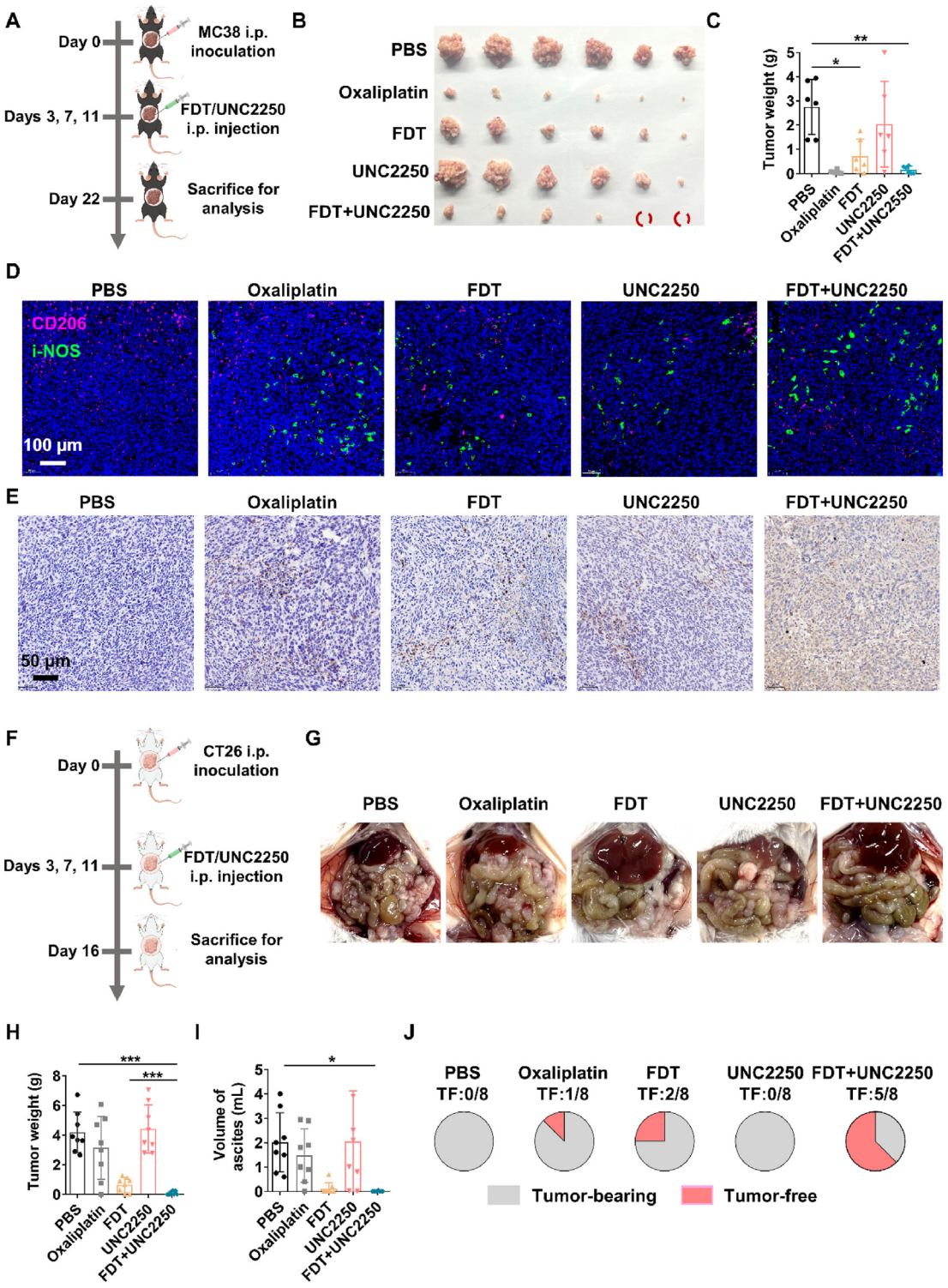

Figure 5 The combinational strategy of FDT and MerTK inhibitor could further promote tumor inhibition. (A) Schematic illustration of combinational regimen for MC38 peritoneal carcinomatosis. (B) Tumor images and (C) the average tumor weights of MC38 peritoneal carcinomatosis in different groups ($n = 6$). Representative images of (D) M1/M2 phenotype TAMs and (E) cleaved-caspase3^{+} cells within the tumor (scale bar = 100 μm and 50 μm). (F) Schematic illustration of combinational regimen for CT26 peritoneal carcinomatosis. (G) Representative images of peritoneal tumors in different groups. (H) The average tumor weights and (I) ascites volume and (J) tumor-free rate of CT26 peritoneal carcinomatosis in different groups ($n = 8$). Note: the red circle represents tumor-free. Diagrammatic drawings in (A) and (F) were created by Figdraw. Data are presented as mean ± SD. *$P < 0.05$, **$P < 0.01$, ***$P < 0.001$.

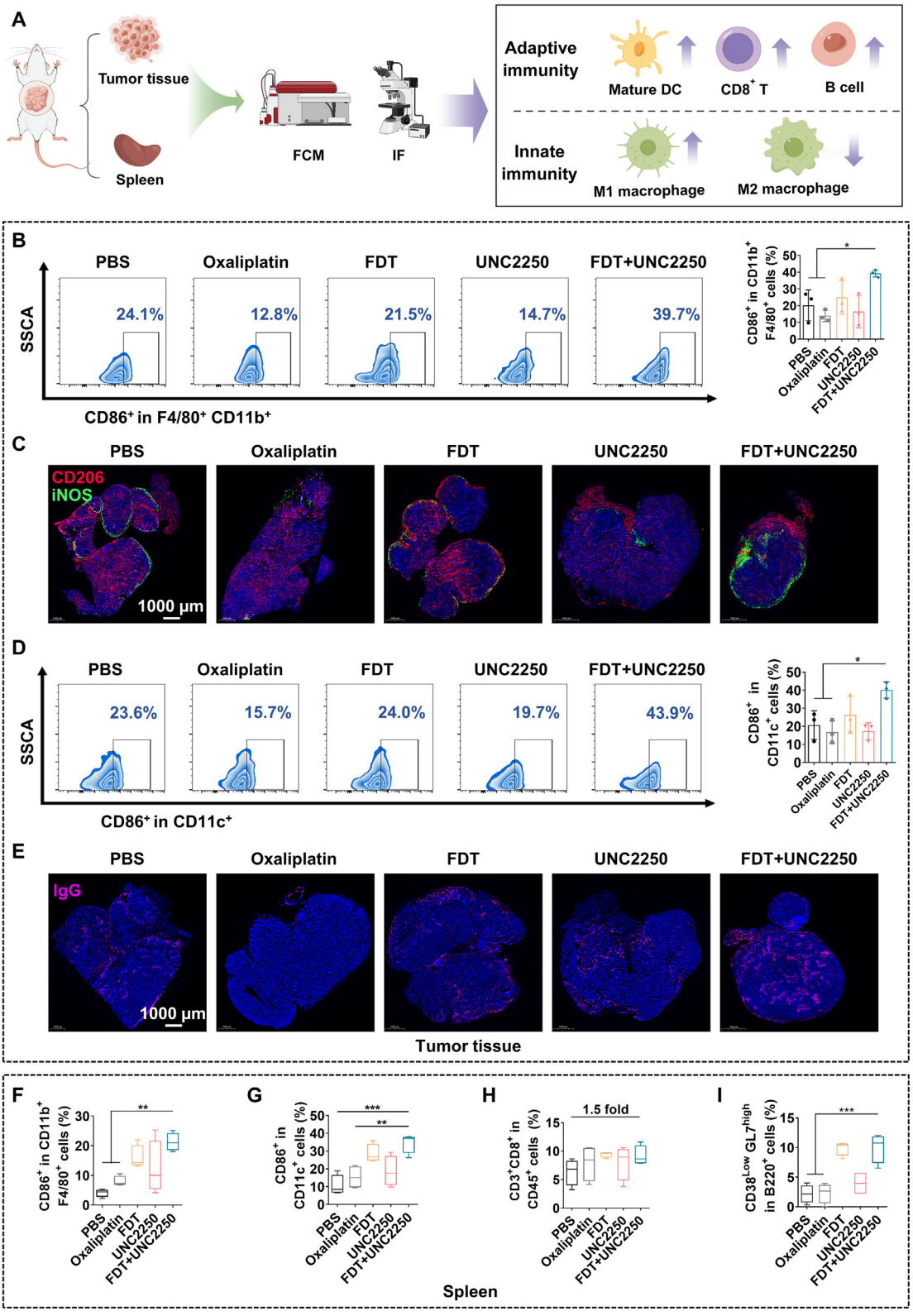

Figure 6 The combination therapy can boost adaptive and innate immunity simultaneously. (A) Schematic illustration of flow cytometry analysis and immune fluorescence observation of tumor tissue and spleen. (B) Quantitative analysis and representative flow cytometry plots of M1 phenotype TAMs ($CD86^+$ in $CD11b^+$ $F4/80^+$) within tumor. (C) Immunofluorescence images of M1/M2 phenotype TAMs within the tumor (scale bar 1000 μm). (D) Quantitative analysis and representative flow cytometry plots of matured DCs ($CD86^+$ in $CD11c^+$) within the tumor ($n = 3$). (E) Immunofluorescence images of IgG expression within the tumor (scale bar 1000 μm). Quantitative analysis of (F) M1 phenotype macrophages ($CD86^+$ in $CD11b^+$ $F4/80^+$), (G) mature DC ($CD86^+$ in $CD11c^+$), (H) $CD8^+$ T lymphocytes ($CD3^+$ $CD8^+$ in $CD45^+$) and (I) germinal center B lymphocytes ($CD38^{Low}$ $GL7^{High}$ in $B220^+$) within spleen ($n = 4$). The diagrammatic drawing in (A) was created by Figdraw. Data are presented as mean ± SD. $^*P < 0.05$, $^{**}P < 0.01$, $^{***}P < 0.001$.

successful immune activation of macrophages in the immune organ induced by this combinational strategy. This combinational strategy further activated DCs in the spleen (Fig. 6G; Fig. S11B), resulting in the highest portion of $CD8^+$ T lymphocytes in the spleens (Fig. 6H; Fig. S11C). In addition, the combinational treatment further boosted the proliferation of germinal center B lymphocytes (GCB, $CD38^{Low}$ $GL7^{High}$) in the spleen compared with FDT monotherapy (Fig. 6I; Fig. S11D), suggesting the activation of germinal center in lymphoid tissue. Overall, these findings illustrated that the combination of FDT and UNC2250 could trigger M1-like polarization of TAMs and the activation of DCs simultaneously, thus eliciting cooperative activation of adaptive immunity and innate immunity.

4. Discussion

The use of X-radiation to induce ICD in tumor cells has been proven to be effective in activating the immune system. Over the years, most clinical research has focused on developing a potent *in situ* cancer vaccine *via* X-radiation. Recent research has proved that repeated low-dose radiation can elicit stronger type I interferon response of *in situ* tumor cells compared with single high-dose radiation[17]. Besides local radiation, researchers also found that total body irradiation can result in massive infiltration of T cells and subsequent tumor eradication[38]. Although these findings provide a favorable basis for the development of X-ray-induced *in situ* vaccines, the effectiveness of these *in situ* vaccines induced by X-radiation is still far from clinical demand due to the limitation of the maximum permissible dose. In contrast, direct irradiation of tumor cells *in vitro* allows higher radiation doses without damaging normal tissue, making it a more feasible method for DTC preparation. Therefore, in this study, we chose X-Ray as an ICD inducer to build a vaccine system with high immunogenicity.

However, the relationship between *in vitro* irradiation dose and immunogenicity of DTC remained unclear. We thereby explored the dose-response relationship between radiation and immunogenicity of the FDT vaccine. And finally, we figured out the positive correlation between radiation dose and immunogenicity. Based on this conclusion, we optimized the radiation dose during FDT preparation, thereby facilitating superior tumor inhibition in metastatic colon cancer. This was particularly significant in the treatment of peritoneal carcinomatosis in colon cancer, which was always associated with poor overall prognosis[2]. FDT effectively inhibited rapid metastasis of cancer cells accompanied by the accumulation of malignant ascites. Even for the MSS type CT26 model that was almost intractable for oxaliplatin, FDT also showed superior antitumor effects. Notably, the FDT vaccine can induce robust type I interferon response *via* STING signaling in DCs due to high-dose radiation-induced accumulation of intracellular dsDNA. Consistently, FDT activated DCs within the tumor, thus eliciting strong tumor-specific T lymphocyte immune response and B lymphocyte immune response.

Although FDT can induce strong activation of DCs, macrophages were unresponsive in FDT-treated mice. The primary factor was that TAMs could recognize and bind with PS on FDT *via* the recognition of MerTK, thereby triggering immune clearance to maintain immunosuppression in TME. Given that massive exposure of PS on FDT can be recognized as an 'eat me' signal *via* the MerTK receptor on macrophages, we next combined FDT with MerTK inhibitor UNC2250 to avoid the immune clearance of FDT and apoptotic tumor cells by TAMs, thus restoring effective M1-like polarization of macrophages. As expected, this combinational strategy significantly reduced the engulfment of FDT by macrophages. In TME, the MerTK blockade *via* UNC2250 substantially reduced the FDT internalization by TAMs specifically. In addition, there was a noticeable increase in apoptosis within the tumor tissue after combinational treatment, indicating rapid accumulation of apoptotic cells. With the inhibition of FDT clearance, the combination of FDT and UNC2250 could activate the STING signaling in macrophages effectively and lead to enhanced M1-like repolarization of TAMs, indicating an effective activation of innate immunity. Besides, DCs were further activated by inhibiting the immunosuppressive clearance medicated by TAMs. Thereby, the $CD8^+$T lymphocytes and B lymphocytes were further enhanced compared with the FDT monotherapy, indicating the enhancement of DCs-mediated adaptive immunity induced by this combinational treatment. Consequently, this combinational strategy evoked much stronger tumor-specific immunity than FDT monotherapy, thus further enhancing the tumor inhibition compared with FDT treatment.

5. Conclusions

In summary, we have proposed a safe and effective cancer vaccine strategy by combining X radiation-induced FDT vaccine with the macrophage efferocytosis checkpoint inhibitor UNC2250. This novel vaccine strategy integrated high immunogenicity and low safety risk. In the future, the FDT vaccine could be prepared from the tumor tissue excised from individual patients, which can retain favorable therapeutic effects and be easy to preserve, thus providing an innovative idea for the development and translation of personalized cancer vaccines.

Acknowledgments

This research was supported by the National Natural Science Foundation of China (No. 82104098, China), the Program for HUST Academic Frontier Youth Team (No. 2018QYTD13, China), Wuhan Science and Technology Plan (2022023702025187, China) and Natural Science Foundation of Hubei Province (2023AFD152, China). We appreciate the scanning electron microscopy analysis provided by the Analytical and Testing Center of Huazhong University of Science and Technology, FCM analysis provided by Medical sub-center of analytical and testing center, Huazhong University of Science and Technology and animal care provided by Laboratory Animal Center of Huazhong University of Science and Technology.

Author contributions

Hongbo Xu, Xianya Qin, Conglian Yang, and Zhiping Zhang conceived the project and designed the experiments. Hongbo Xu, Xianya Qin, Runzan Zhang, Siyu Zhao, Tianyi Tian, Yuanyuan Guo, and Xingxing Feng performed the experiments. Hongbo Xu, Conglian Yang, Li Kong, and Zhiping Zhang helped with critical data analysis and wrote the manuscript. All authors discussed the results and approved the final version of the manuscript.

Conflicts of interest

The authors declare no conflicts of interest.

Appendix A. Supporting information

Supporting data to this article can be found online at https://doi.org/10.1016/j.apsb.2024.02.015.

References

1. Franko J, Shi Q, Meyers JP, Maughan TS, Adams RA, Seymour MT, et al. Prognosis of patients with peritoneal metastatic colorectal cancer given systemic therapy: an analysis of individual patient data from prospective randomized trials from the analysis and research in cancers of the digestive system (ARCAD) database. *Lancet Oncol* 2016;**17**:1709−19.
2. Cortes-Guiral D, Hubner M, Alyami M, Bhatt A, Ceelen W, Glehen O, et al. Primary and metastatic peritoneal surface malignancies. *Nat Rev Dis Prim* 2021;**7**:92.
3. Kepenekian V, Bhatt A, Peron J, Alyami M, Benzerdjeb N, Bakrin N, et al. Advances in the management of peritoneal malignancies. *Nat Rev Clin Oncol* 2022;**19**:698−718.
4. Harper MM, Kim J, Pandalai PK. Current trends in cytoreductive surgery (CRS) and hyperthermic intraperitoneal chemotherapy (HIPEC) for peritoneal disease from appendiceal and colorectal malignancies. *J Clin Med* 2022;**11**:2840.
5. Kopetz S. New therapies and insights into the changing landscape of colorectal cancer. *Nature Nat Rev Gastroenterol Hepatol* 2019;**16**:79−80.
6. Guinney J, Dienstmann R, Wang X, Reyniès AD, Schlicker A, Soneson C, et al. The consensus molecular subtypes of colorectal cancer. *Nat Med* 2015;**21**:1350−6.
7. Noh I, Son YJ, Jung W, Kim M, Kim DY, Shin HC, et al. Targeting the tumor microenvironment with amphiphilic near-infrared cyanine nanoparticles for potentiated photothermal immunotherapy. *Biomaterials* 2021;**275**:120926.
8. Wang ZR, Li WP, Park JH, Gonzalez KM, Scott AJ, Lu JQ, et al. Camptothesome elicits immunogenic cell death to boost colorectal cancer immune checkpoint blockade. *J Control Release* 2022;**349**:929−39.
9. Qin XY, Yang T, Xu HB, Zhang RZ, Zhao SY, Kong L, et al. Dying tumor cells-inspired vaccine for boosting humoral and cellular immunity against cancer. *J Control Release* 2023;**359**:359−72.
10. Deng LF, Liang H, Xu M, Yang XM, Burnette B, Arina A, et al. STING-dependent cytosolic DNA sensing promotes radiation-induced type I interferon-dependent antitumor immunity in immunogenic tumors. *Immunity* 2014;**41**:843−52.
11. Woo SR, Fuertes MB, Corrales L, Spranger S, Furdyna MJ, Leung MYK, et al. STING-dependent cytosolic DNA sensing mediates innate immune recognition of immunogenic tumors. *Immunity* 2014;**41**:830−42.
12. Barber GN. STING: infection, inflammation and cancer. *Nat Rev Immunol* 2015;**15**:760−70.
13. Motwani M, Pesiridis S, Fitzgerald KA. DNA sensing by the cGAS-STING pathway in health and disease. *Nat Rev Genet* 2019;**20**:657−74.
14. Vanpouille-Box C, Alard A, Aryankalayil MJ, Sarfraz Y, Diamond JM, Schneider RJ, et al. DNA exonuclease Trex1 regulates radiotherapy-induced tumor immunogenicity. *Nat Commun* 2017;**8**:15618.
15. Zizzo G, Hilliard BA, Monestier M, Cohen PL. Efficient clearance of early apoptotic cells by human macrophages requires M2c polarization and MerTK induction. *J Immunol* 2012;**189**:3508−20.
16. Zhou Y, Fei MJ, Zhang G, Liang WC, Lin WY, Wu Y, et al. Blockade of the phagocytic receptor MerTK on tumor-associated macrophages enhances P2X7R-dependent STING activation by tumor-derived cGAMP. *Immunity* 2020;**52**:357−373.e9.
17. Wang QW, Bergholz JS, Ding LY, Lin ZY, Kabraji SK, Hughes ME, et al. STING agonism reprograms tumor-associated macrophages and overcomes resistance to PARP inhibition in BRCA1-deficient models of breast cancer. *Nat Commun* 2022;**13**:3022.
18. Chabanon RM, Rouanne M, Lord CJ, Soria JC, Pasero P, Postel-Vinay S. Targeting the DNA damage response in immuno-oncology: developments and opportunities. *Nat Rev Cancer* 2021;**21**:701−17.
19. Galluzzi L, Buqué A, Kepp O, Zitvogel L, Kroemer G. Immunogenic cell death in cancer and infectious disease. *Nat Rev Immunol* 2017;**17**:97−111.
20. Li QQ, Shi ZQ, Zhang F, Zeng WW, Zhu DW, Mei L. Symphony of nanomaterials and immunotherapy based on the cancer-immunity cycle. *Acta Pharm Sin B* 2022;**12**:107−34.
21. Lin YX, Wang Y, Ding JX, Jiang AP, Wang J, Yu M, et al. Reactivation of the tumor suppressor PTEN by mRNA nanoparticles enhances antitumor immunity in preclinical models. *Sci Transl Med* 2021;**13**:eaba9772.
22. Yu YK, Cheng QZ, Ji XY, Cheng HZ, Zeng WF, Zeng XW, et al. Engineered drug-loaded cellular membrane nanovesicles for efficient treatment of postsurgical cancer recurrence and metastasis. *Sci Adv* 2022;**8**:eadd3599.
23. Ci TY, Li HJ, Chen GJ, Wang ZJ, Wang JQ, Abdou P, et al. Cryo-shocked cancer cells for targeted drug delivery and vaccination. *Sci Adv* 2020;**6**:7.
24. Obeid M, Tesniere A, Ghiringhelli F, Fimia GM, Apetoh L, Perfettini JL, et al. Calreticulin exposure dictates the immunogenicity of cancer cell death. *Nat Med* 2007;**13**:54−61.
25. Kroemer G, Galluzzi L, Kepp O, Zitvogel L. Immunogenic cell death in cancer therapy. *Annu Rev Immunol* 2013;**31**:51−72.
26. Hegde PS, Chen DS. Top 10 challenges in cancer immunotherapy. *Immunity* 2020;**52**:17−35.
27. Qin XY, Yang CL, Xu HB, Zhang RZ, Zhang D, Tu JY, et al. Cell-derived biogenetic gold nanoparticles for sensitizing radiotherapy and boosting immune response against cancer. *Small* 2021;**17**:e2103984.
28. Zhang D, Wu TT, Qin XY, Qiao Q, Shang LH, Song QL, et al. Intracellularly generated immunological gold nanoparticles for combinatorial photothermal therapy and immunotherapy against tumor. *Nano Lett* 2019;**19**:6635−46.
29. Alloatti A, Kotsias F, Magalhaes JG, Amigorena S. Dendritic cell maturation and cross-presentation: timing matters. *Immunol Rev* 2016;**272**:97−108.
30. Jhunjhunwala S, Hammer S, Delamarre L. Antigen presentation in cancer: insights into tumor immunogenicity and immune evasion. *Nat Rev Cancer* 2021;**21**:298−312.
31. Mekers VE, Kho VM, Ansems M, Adema GJ. cGAS/cGAMP/STING signal propagation in the tumor microenvironment: key role for myeloid cells in antitumor immunity. *Radiother Oncol* 2022;**174**:158−67.
32. Nishi C, Yanagihashi YC, Segawa K, Nagata S. MERTK tyrosine kinase receptor together with TIM4 phosphatidylserine receptor mediates distinct signal transduction pathways for efferocytosis and cell proliferation. *J Biol Chem* 2019;**294**:7221−30.
33. Yan D, Earp HS, DeRyckere D, Graham DK. Targeting MERTK and AXL in EGFR mutant non-small cell lung cancer. *Cancers* 2021;**13**:26.
34. Myers KV, Amend SR, Pienta KJ. Targeting Tyro3, Axl and MerTK (TAM receptors): implications for macrophages in the tumor microenvironment. *Mol Cancer* 2019;**18**:94.
35. Staff C, Magnusson CGM, Hojjat-Farsangi M, Mosolits S, Liljefors M, Frödin JE, et al. Induction of IgM, IgA and IgE antibodies in colorectal cancer patients vaccinated with a recombinant CEA protein. *J Clin Immunol* 2012;**32**:855−65.
36. Yang B, Zhang Z, Chen XJ, Wang XY, Qin SS, Du LQ, et al. An asia-specific variant of human IgG1 represses colorectal tumorigenesis by shaping the tumor microenvironment. *J Clin Invest* 2022;**132**:e153454.
37. Cabrita R, Lauss M, Sanna A, Donia M, Larsen MS, Mitra S, et al. Tertiary lymphoid structures improve immunotherapy and survival in melanoma. *Nature* 2020;**577**:561−5.
38. Filatenkov A, Baker J, Mueller AMS, Kenkel J, Ahn GO, Dutt S, et al. Ablative tumor radiation can Change the tumor immune cell microenvironment to induce durable complete remissions. *Clin Cancer Res* 2015;**21**:3727−39.